Available online at www.sciencedirect.com
ScienceDirect
International Journal of Thermal Sciences 47 (2008) 1026–1042
International Journal of Thermal Sciences
www.elsevier.com/locate/ijts

Unsteady heat transfer by natural convection in the cavity of a passive heating room

İrfan Kurtbaş *, Aydın Durmuş

Department of Mechanical Education, University of Firat, 23119 Elazığ, Turkey

Received 1 February 2007; received in revised form 3 August 2007; accepted 3 August 2007

Available online 20 September 2007

Abstract

In this study, three dimensional unsteady state equations of heat transfer and flow have been solved numerically for a passive heating room using values of hourly averaged radiation during winter in Elazığ region in Turkey. For this purpose, a room having volume of 44.8 m^3 ($4 \times 4 \times 2.8$ m) was considered. Variable heat flux boundary condition depending on time was applied on absorber surface using values of hourly averaged radiation. Convection boundary condition was used on glass surface, the walls and ceiling of the room by using overall heat transfer coefficient. Constant surface temperature (6 °C) was used for floor of the room. Experiments were carried out manufacturing a model room having the size of $1 \times 1.2 \times 1.2$ m dimensions in order to maintain the corroboration of numerical solution. Governing equations for the model room built were solved numerically and compared to experimental data. It was seen that the model predictions agreed quite well with experimental data. The effect of overall heat transfer coefficient of glass on Nusselt number was also investigated. It was revealed that the overall heat transfer coefficient for low Rayleigh number affected the average Nusselt number more than that of high Rayleigh number.

Keywords: Passive heating; Solar energy; Numerical solution; Variable heat flux

1. Introduction

For heating of buildings using solar energy, the solar energy is collected and distributed properly in space by using either effective or passive ventilation. If ventilation is provided by systems based on mechanical components that consume electric power, the system is called as effective ventilation (or active system). Otherwise, the system is called as passive ventilation (or passive solar heating) based on natural convection. There are four passive heating system approaches: (i) sun-tempering which is achieved through modest increases in south-facing windows; (ii) insolated gain involving passively capturing solar heat and then moving it passively into or out of the building using a liquid or air; (iii) direct gain which is one of the most basic forms of passive solar heating. In this system, sunlight enters the space to be heated, and is stored in a thermal mass incorporated into the floor or interior walls; (iv) indirect gain (also called a Trombe wall or thermal storage wall), in which solar radiation is captured by a part of the building envelope designed with an appropriate thermal mass; such as a solid concrete or a masonry wall or a water tank behind glass. Thermal storage wall is also called as massive thermal wall.

Passive solar heating is widely used in the cold climates. Passive design requires a detailed profound knowledge of energy and heat flow behavior in the considered structure [1]. In order to determine the energy performance of buildings, the most reliable numerical models are based on time-dependent solutions of energy and momentum equations.

Different investigations using either solar passive cooling systems (SPCS) or solar passive heating systems (SPHS) for thermal comfort conditions of buildings have been performed in previous studies. Those investigations contain either the experimental study or numerical solution or both of them. Possibilities and limitations of natural ventilation in restored industrial building with a double-skin façade and effect of fixed horizontal louver shading devices on thermal performance of buildings

* Corresponding author. Tel.: +90 424 2370000; fax: +90 424 2367064.
E-mail addresses: ikurtbas@gmail.com (İ. Kurtbaş), adurmus1@firat.edu.tr (A. Durmuş).

1290-0729/$ – see front matter
doi:10.1016/j.ijthermalsci.2007.08.001

Nomenclature

A	area	m^2
g	gravitational acceleration	$m\,s^{-2}$
h	static enthalpy	$J\,kg^{-1}$
h_w	convection coefficient of the environment	$W\,m^{-2}\,K^{-1}$
k	thermal conductivity of the air	$W\,m^{-1}\,K^{-1}$
Nu	Nusselt number	
P	static pressure	Pa
P'	modified pressure	Pa
q	heat flux	$W\,m^{-2}$
Q	heat	W
Ra	modified Rayleigh number based on the heat flux and the cavity width	
Ra_Y	modified Rayleigh number based on the cavity height	
R	regression coefficient	
S	the cavity width	m
t	time	s, h
T	temperature	°C, K
U	overall heat transfer coefficient	$W\,m^{-2}\,K^{-1}$
u	velocity in x direction	$m\,s^{-1}$
v	velocity in y direction	$m\,s^{-1}$
V_w	wind velocity	$m\,s^{-1}$
w	velocity in z direction	$m\,s^{-1}$
x, y, z	Cartesian coordinate	

Greek symbols

α	thermal diffusivity	$m^2\,s^{-1}$
β	expansion coefficient	K^{-1}
ε	emissivities	
θ	dimensionless temperature	
ρ	density	$kg\,m^{-3}$
σ	Stefan–Boltzmann constant, $5.67 \times 10^{-8}\,W\,m^{-2}\,K^{-4}$	
τ	stress tensor	$N\,m^{-2}$
υ	kinematics viscosity of the air	$m^2\,s^{-1}$

Subscripts

a	absorber
c	ceiling
e	environment
f	floor
g	glass
i, j, k	direction
R	radiation
w	wall

were investigated by using TRNSYS program [2,3]. Chen et al. [4] investigated numerically and experimentally the heat transfer and air flow in passive heating room with greenhouse and heat storage systems. Solar chimney and roof solar collectors (RSC) were considered in order to improve the indoor thermal comfort of houses or buildings [5–7]. Many investigators analyzed and solved numerically the natural convection problems in Trombe walls for two dimensional laminar flow and steady state conditions [8–10]. A theoretical study has been presented including combined heat transfer by conduction, convection and radiation in a rectangular cavity by Hasnaoui et al. [11]. Demirbilek et al. [12] have tested thermal performance of a building, and evaluated through different modes of application of insulation, materials, type of glazing, window/wall ratios. Gan [13] and Rincon et al. [14] have evaluated numerically the thermal performance of a solar passive cooling system under a hot and humid climate. In another work, the flow and temperature fields in terms of temperature and velocity distributions at the exit section of duct of a heated vertical channel has been presented numerically [15].

Although the experimental and numerical energy savings have been widely reported for the passive heating system, very few papers have presented local heat and velocity distribution in the cavity. These papers have presented the heat and fluid flow for two dimensional and steady state conditions. However, the numerical method adopted in this work includes the solution of three dimensional unsteady state momentum and energy equations.

2. Problem description and physical model

2.1. System description

The basic model of a passively ventilated room is illustrated in Fig. 1. The interior dimensions of the room and cavity are $4.0 \times 2.8 \times 4.0$ m and $4.0 \times 2.8 \times 0.2$ m, respectively. The cavity is basically composed of two parallel plates forming a vertical channel in which the air can circulate. The internal wall (south wall of the heating room) is an absorber of 0.3 m thickness. The solar absorber wall (SAW), in which ten vents have been drilled to be equal number on the top and bottom sides, is designed to directly gain solar heat (as shown in Fig. 1). The external wall is a double glass. It has been assumed that all walls except top and bottom walls are made of masonry brick of 0.3 m thickness. Besides, all of the six walls are insulated in the middle of the walls by glass wool of 0.05 m thickness, which has low thermal conductivity ($k_1 = 0.038\,W\,m^{-1}\,K^{-1}$). The top and bottom walls are made of concrete having 2200 $kg\,m^{-3}$ density and 1.75 $W\,m^{-1}\,K^{-1}$ thermal conductivity.

2.2. Numerical procedure

Using Fluent 5.5 Computational Fluid Dynamics (CFD) software, the basic conservation equations were solved numerically. Natural convection problems demand on the simultaneous solution of the conservation equations of momentum, mass and enthalpy [16]. The numerical calculations were performed for the unsteady velocity and temperature fields inside the room

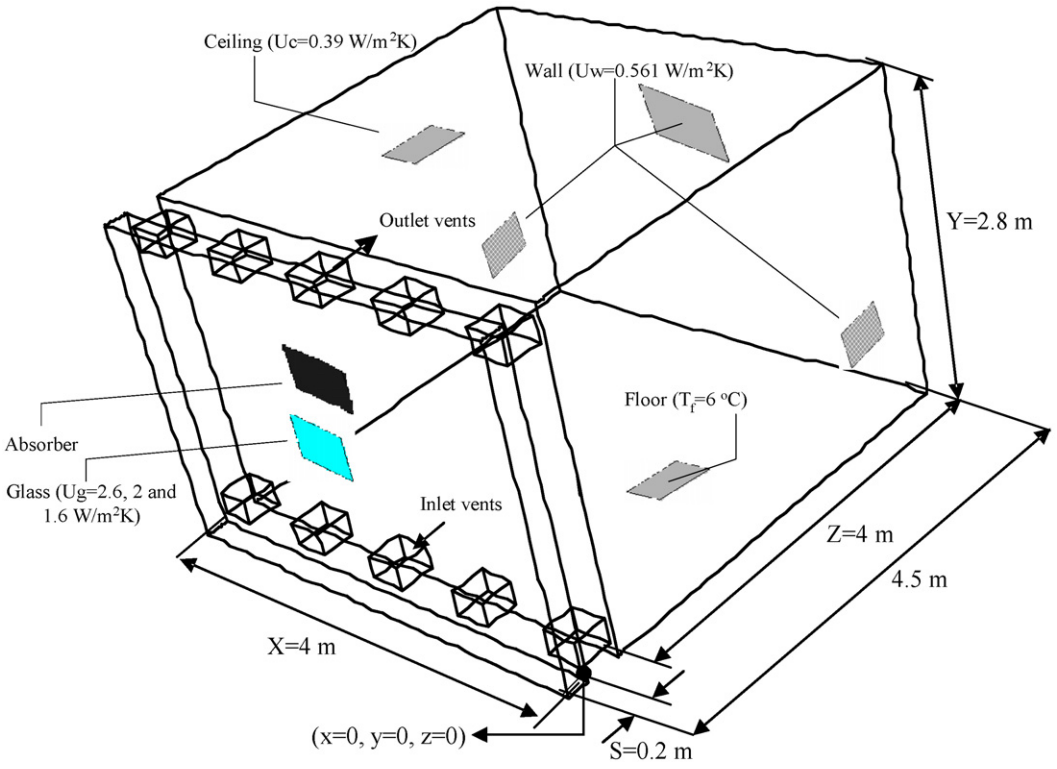

Fig. 1. The basic model for the room.

and the cavity. The equations for continuity and velocity components take the following forms:

- *Continuity equation*

$$\frac{\partial \rho}{\partial t} + \frac{\partial}{\partial x_i}(\rho u_i) = 0 \tag{1}$$

- *Momentum equation*

$$\frac{\partial}{\partial t}(\rho u_i) + \frac{\partial}{\partial x_i}(\rho u_i u_j) = -\frac{\partial P}{\partial x_i} + \frac{\partial \tau_{ij}}{\partial x_j} + \rho g_i \tag{2}$$

- *Energy equation*

$$\frac{\partial}{\partial t}(\rho h) + \frac{\partial}{\partial x_i}(\rho u_i h) = u_i \frac{\partial P}{\partial x_i} + \frac{\partial}{\partial x_i}\left(k \frac{\partial T}{\partial x_i}\right) + \tau_{ij} \frac{\partial \tau_i}{\partial x_j} \tag{3}$$

where t is the time, ρ is the density, u_i is the velocity component in the i-direction, P is the static pressure, x_i is a Cartesian coordinate, τ_{ij} is the stress tensor, g_i is the gravitational acceleration in the i-direction, h is the static enthalpy, k is the thermal conductivity of working fluid and T is the temperature. The following assumptions are considered for calculating the governing equations.

- The flow is considered as laminar, unsteady and three dimensional.
- The fluid is Newtonian.
- Thermophysical properties of the fluid are constant except for the density change with temperature which gives rise to the buoyancy forces.
- The viscous dissipation is negligible.
- Heat is transferred from the SAW by convection to the flowing air and by radiation to the cavity walls, as the glass and the SAW emissivities are not negligible.
- Boussinesq approximation for the treatment of the natural convection of the air contained in the interior of the cavity is used.

2.3. Boundary and initial conditions

- No-slip at all boundaries.
- Pressure (P') is zero at all openings of the cavity. Since the flow is buoyancy-driven, Eq. (2) for vertical direction is redefined in Fluent using the relation of $P' = -\rho_o g y + P$, in which ρ_o is the reference density taken at 300 K and atmospheric pressure [18,19].
- The air in the room and the cavity is initially stagnant and at a uniform temperature (6 °C) which differs from the environment temperature.
- The environment temperature is assumed uniform (0 °C) for all cases.
- It is assumed that the SAW is insulated on the side of the room, and is painted black on the side of the cavity where solar radiation is absorbed.

The boundary conditions used in the system are clearly depicted in Fig. 1. The surface-to-surface radiation was taken into account through the so-called Discrete Transfer Radiation Model (DTRM). The DTRM assumes that all surfaces are diffuse, i.e. the reflection of incident radiation at the surface is isotropic with respect to solid angle [16]. In this connection,

the emissivities of the glass, black surface (SAW) and the walls (painted white color) were used as $\varepsilon_g = 0.86$, $\varepsilon_a = 0.93$ and $\varepsilon_w = 0.91$, respectively as given in Ref. [20]. Heat transfer occurs by convection, for the boundary conditions on all of the vertical surfaces, and on the top surface. If the environment temperature is provided, then the overall heat transfer coefficient (U) incorporated in the computations consists of both thermal conductivity of the wall and convection coefficient of the environment, which is obtained by relationship of $h_w = 5.6 + 3.8V_w$ [20]. In the present study, it is assumed that wind velocity (V_w) is constant, and consequently, convection coefficient of the environment (h_w) does not change during daytime. A uniform temperature boundary condition is used on the bottom surface.

As known, incident solar radiation changes depending on time of the day. In this study, hourly average of the solar radiation during the winter months in Elazığ region in Turkey (latitude: 38° 40′; longitude: 39° 39′; altitude: 991 m) was calculated. When the numerical calculations were performed, heat flux boundary condition, which changed depending on time, was used on the SAW. The equations of continuity, energy and momentum were solved considering 15 minute period time. After 15 minutes, the obtained results were considered as the initial conditions of the next time period. Convergence of the solution was checked at each time step, with the convergence criterion of 10^{-4} for velocity components and continuity, and criterion of 10^{-6} for energy. When heat flux value was changed, the temperature and velocity component values obtained in a previous time step for each node were assigned as initial conditions. In this study, for all cases laminar model was used since the modified Rayleigh number including the heat flux (q) and width of the cavity (S) was less than 1×10^9. Although the modified Rayleigh number increased up to 1.1×10^9 at 12 am, for a short time period, still laminar model was considered.

The cavity was filled a non-uniform grid with a very fine spacing near the walls, as needed for accurately resolving the steep gradients in the thin buoyancy-driven boundary layer. However, regular grid was applied in the room. The overall number of cells in the room including the cavity and the vents are 68.013. Letan et al. performed a similar study in terms of methods used [16,17]. They investigated a multi-storey structure in their study. They used 70 000 cells for each storey of the structure, and the overall number of cells in the system was about 300 000, including the duct and ports. As can be seen in Table 1, the grid number did not affect the flow field inside the enclosure significantly. For instance, increasing grid number from 68 013 to 98 331 had no important effect on flow behavior, but considering the later grid number, the computational time was approximately two times longer than the former one.

Table 1
Comparisons of local Nusselt number for various grid arrangements for $Ra = 1.6 \times 10^8$ (8 am), $U_g = 2.6\ \mathrm{W\,m^{-2}\,K^{-1}}$ and $T_e = 0\,^\circ\mathrm{C}$

Grid number	x (at $y = 1.4$ m)		
	0.1 m	1 m	2 m
47 381	23.27	23.21	22.91
68 013	22.83	22.01	21.88
98 331	22.07	21.84	21.60

2.4. Validation of the computations

The numerical computation is verified with experimental data. A model passive heating system (MPHS) was built to validate the numerical procedure by a comparison with the experimental data, which included the temperatures on the glass, and the velocity measurements in the cavity of MPHS. Inner and outer surfaces of MPHS's walls, which were made of standard bricks and insulation materials, were coated by a plaster with a thick of 0.02 m. The cavity in the MPHS has the inner length, width and height of 1 m, 0.2 m and 0.8 m, respectively. Front side of the MPHS was closed by standard double-glass of 12 mm thickness in total (each glass is 3 mm and void space is 6 mm). As shown in Fig. 2(a), the structure geometry of MPHS is different from the real-size geometry. The reason for this difference was to make a comparison between Trombe wall and thermosiphon system for the same value of the solar radiation. Therefore, a MPHS with both vertical and tilted (38°) surface was built. In this way, a performance evaluation of the passive heating system with Trombe wall and thermosiphon system was carried out. But, more detail will be given further.

T-type thermocouples of 0.5 mm diameter were placed on the surface of the glazing and the SAW in the cavity. The airflow velocity was measured with an ALMEMO Thermoelectric Flow Sensor (FVA605TA1 Model). The velocity and temperature measurements were both collected and recorded by a computer aided data-logger (ALMEMO 5990-0 Model). The accuracies of the anemometer and the thermocouples were ±1–1.5% and ±0.1% of full-scale, respectively.

The velocity of the air was measured setting the anemometer in the centre of the cavity considering two different distances from the bottom of the cavity ($y = 0.25$ and $y = 0.45$ m). The experiments of the velocity together with the temperatures were performed simultaneously on three and four days for the height of 0.25 and 0.45 m, respectively. As shown in Fig. 2(b), two holes of 12 mm diameter have been drilled in order to fix the anemometer on the left side of the cavity. Using the data concerning different days, an evaluation between numerical and experimental results has been performed. After favorable solution algorithms were determined, these algorithms were used for the room depicted in Fig. 1. As seen in Fig. 3(a), comparison of the predicted and observed temperatures shows a good agreement (especially between 8 am and 17 pm). From the numerical and experimental results (see Fig. 3(a)), it is seen that there is a mean temperature difference up to 90% between 6:45 and 8 am, for 12 April, 2005. This case can be explained by the differences between numerical and experimental initial-boundary conditions; such as uniform temperature distribution and especially shading in the cavity. The temperature differences between predicted and experimental SAW are in the range of 6% at 8.15 am. It is seen that the average SAW temperature obtained by numerical calculations shows a continuous rise and

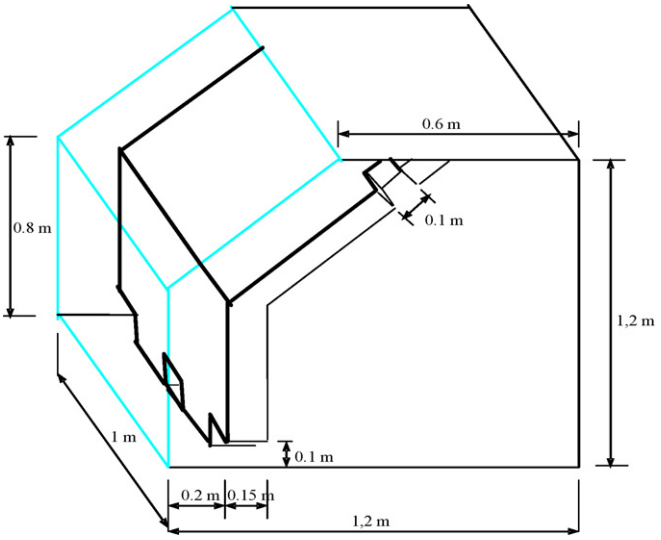

(a)

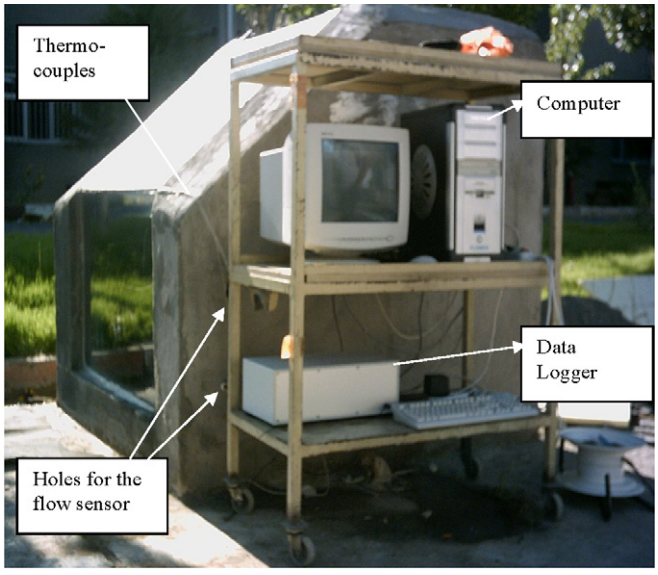

(b)

Fig. 2. (a) Model passive heating system built for the experiments. (b) Experimental set-up.

exceeds in the range of 5–12% the experimental average temperature.

Changing of the experimental and predicted average air velocity with the daytime is given in Fig. 3(b) for $y = 0.25$ and 0.45 m. When numerical calculations were performed, the radiation values obtained from the experiments were used as heat flux on the SAW. Certain deviations occurred between the experimental and predicted average velocity data. The deviations between the experimental and predicted velocities were not same for the selected daytime, i.e. while there was a deviation up to 35.2% at between 6.45 and 8 am, the deviations were in the range of 2–18% between 8 am and 17 pm. Nevertheless, this difference for $y = 0.45$ m started in the range of 45% and continuously reduced up to 0.3% at 13.30 pm (on 14 April 2005).

The experimental results are useful not only for determining the velocities and temperatures in the cavity, but also for providing information about the accuracy of the numerical calculations. It can be observed that the trend of the simulation curves is similar to the experimental results, and agreement is rather good (with maximum ±10% accuracy), except for during the sunrise and sundown.

3. Results and discussions

As it is known, the modified Rayleigh number is one of the important model parameters for a given flow geometry [21,22]. In this study, the modified Rayleigh number including heat flux and the width of the cavity was used, and written as

$$Ra = \frac{g.\beta.q.S^4}{k.\alpha.\upsilon} \tag{4}$$

where g is gravitational acceleration, q is the heat flux on SAW, S is the cavity width, β is thermal expansion coefficient, k is thermal conductivity and υ is kinematic viscosity of the air. The heat transfer characteristics are described by the Nusselt number with its definition as follows:

$$Nu_{(i,k)} = \frac{q.S}{(T_{(i,j)}|_{z=0} - T_{g(i,j)}).k} = \frac{1}{\theta|_{z=0}} \tag{5}$$

the average Nusselt number:

$$Nu = \frac{q.S}{k} \frac{1}{\frac{1}{A}.\int_A (T_{(i,j)}|_{z=0} - T_{g(i,j)}).\mathrm{d}A} = \frac{1}{\frac{1}{A}.\int_A \theta|_{z=0}.\mathrm{d}A} \tag{6}$$

where A is area of SAW, T is temperature and θ is non-dimensional temperature and evaluated as

$$\theta = \frac{T - T_g}{\frac{q.S}{k}} \tag{7}$$

According to Eq. (5), the local Nusselt number is inversely proportional to temperature differences $(T_{a(i,j)} - T_{g(i,j)})$ but also directly proportional to heat flux (q) and the cavity width (S). In some previous works, Eq. (5) was used for determining the local Nusselt number in cavity including either Trombe walls or the flow between two plates. While using the mentioned equation for Trombe wall problems, the glass was either insulated or maintained at constant temperature. Considering this aspect, present study is original from the previous works due to including convection heat transfer at the glass.

The changing of temperature difference between the glass and the absorber throughout the cavity height is given in Fig. 4 for $x/X = 0.5$. As seen at 8 am, temperature difference between the glass and the absorber is approximately 2 °C at $y = 0.3$ m. It increases up to 4.08 °C at $y = 0.4$ m and 5.03 °C at $y = 2.4$ m. Then, it decreases up to 1.8 °C at the boundary of outlet vent. At 9 am, temperature difference begins approximately 9 °C and it decreases up to 7.4 °C at the boundary of inlet vent. Thereafter, it decreases again. It is seen that the variations are similar to each other although these have different values. When Eq. (5) and Fig. 4 are taken into consideration, local Nusselt number must be the maximum at $0 \leqslant y \leqslant 0.4$ m and

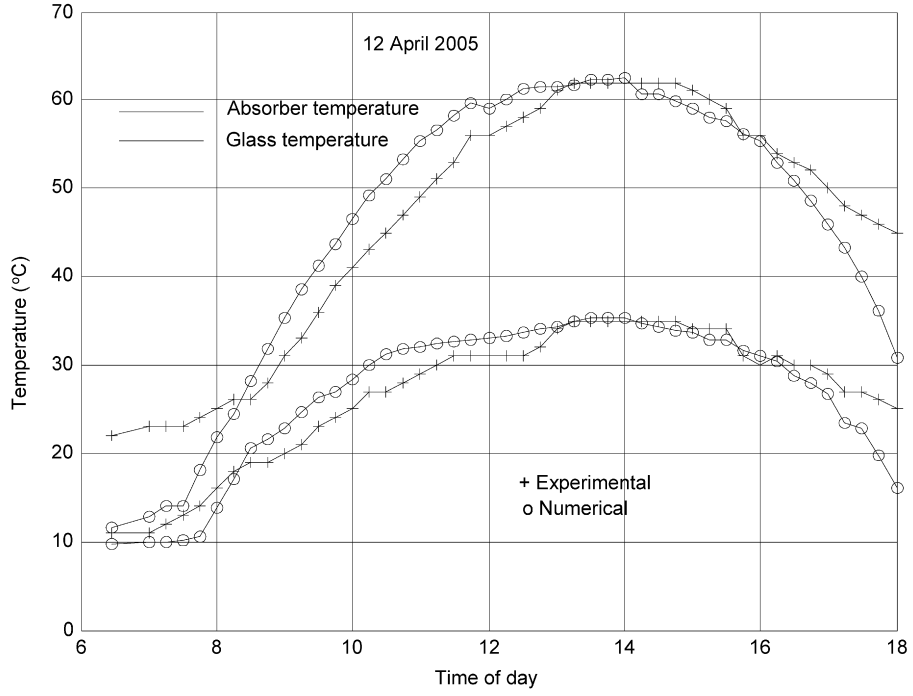

(a)

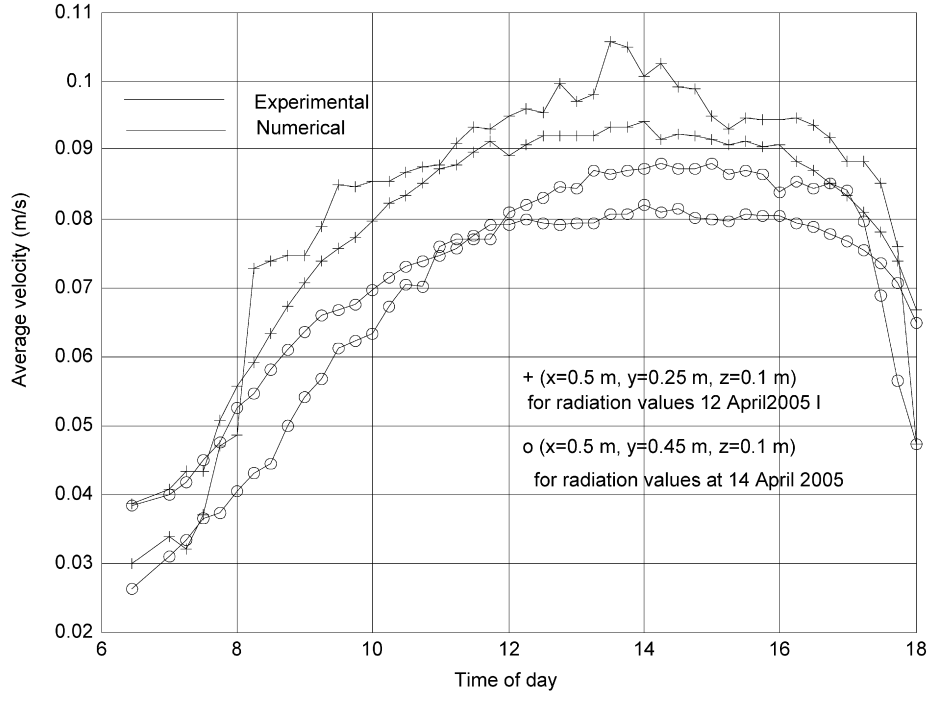

(b)

Fig. 3. (a) Changing of the experimental and numerical temperature with daytime. (b) Changing of the experimental and numerical velocity with daytime.

$2.4 \leqslant y \leqslant 2.8$ m for each time step because minimum temperature difference occurs in that place. Fig. 5(a) shows that local Nusselt number increases approximately up to 52 at boundary of the inlet vents and up to 62 at boundary of the outlet vents. Between inlet and outlet vents, local Nusselt number changes between 22.1 and 24.2. Average heat flux increased 128% level (67.51 W m^{-2}) according to 8 am. The local Nusselt number increased between 54% and 109% at 9 am (Fig. 5(b)), 59.7% and 107.84% at 10 am (Fig. 5(c)). Distribution of the local Nusselt number is given in Fig. 5(d) and 5(e) for 11 am and 12 am, respectively. The maximum local Nusselt number was 226.78 for 11 am and 247.63 for 12 am.

As discussed above, in this study, the flow between the glass and absorber was taken into consideration. The glass and absorber were subjected to convection heat transfer and heat flux, respectively. A few correlations are given in the literature for

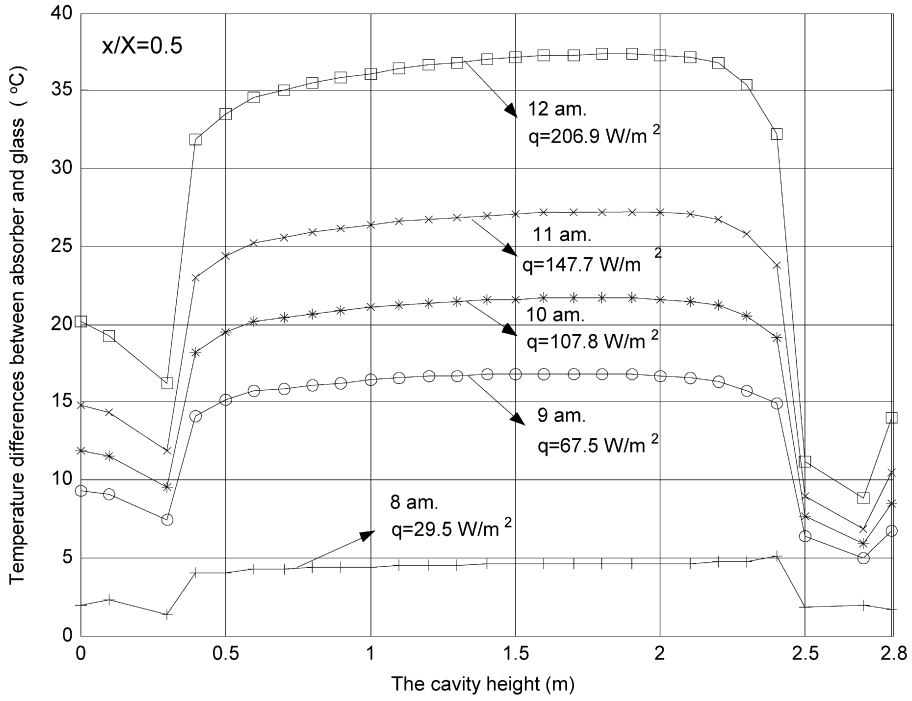

Fig. 4. Changing of temperature differences between the glass and the absorber in the cavity.

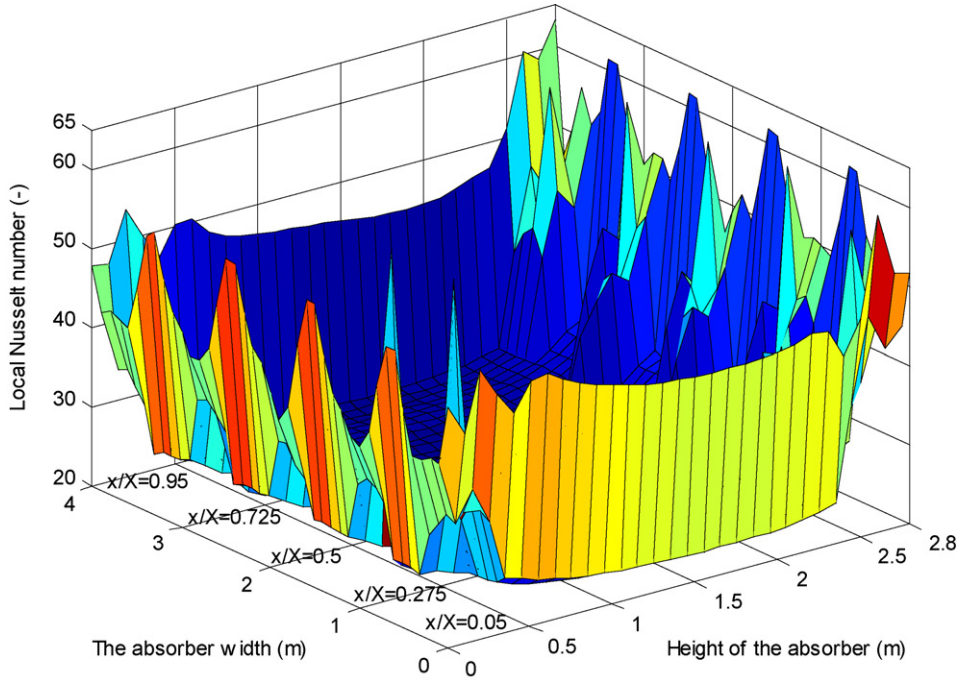

(a)

Fig. 5. Distribution of local Nusselt number in the cavity. (a) for $U_g = 2.6\ \mathrm{W\,m^{-2}\,K^{-1}}$ and 8 am. (b) for $U_g = 2.6\ \mathrm{W\,m^{-2}\,K^{-1}}$ and 9 am. (c) for $U_g = 2.6\ \mathrm{W\,m^{-2}\,K^{-1}}$ and 10 am. (d) for $U_g = 2.6\ \mathrm{W\,m^{-2}\,K^{-1}}$ and 11 am. (e) for $U_g = 2.6\ \mathrm{W\,m^{-2}\,K^{-1}}$ and 12 am.

flow by natural convection between two plates. However, in these correlations, Rayleigh number based on the characteristic length and temperature differences, in general, is considered. Since the modified Rayleigh number including heat flux and the width of the cavity is used in this study, the average Nusselt number is compared to the correlations given by Bar-Cohen and Rohsenow and Fohanno and Polidori [22,23]. The average Nusselt number for both laminar ($Ra < 10^9$) and turbulent flow ($Ra > 10^9$) is given by Bar-Cohen and Rohsenow as $Nu = [(C_1/(Ra.S/Y)) + (C_2/(Ra.S/Y)^{2/5})]^{-1/2}$ for air flow between wall and glass cover [22]. The values of the coefficients C_1 and C_2 are 24 and 2.51, respectively. According

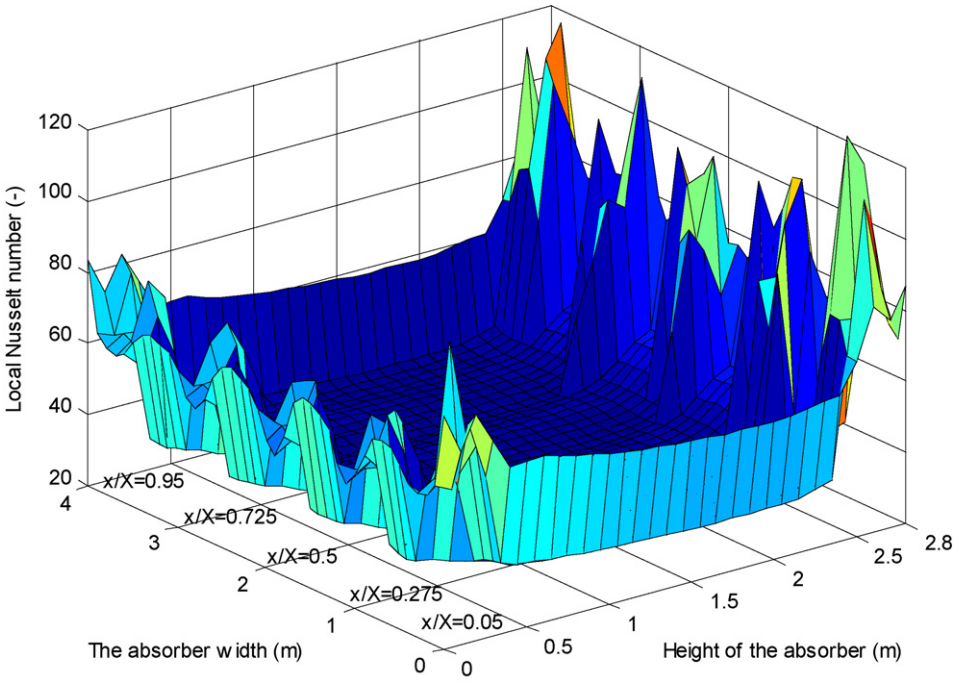

(b)

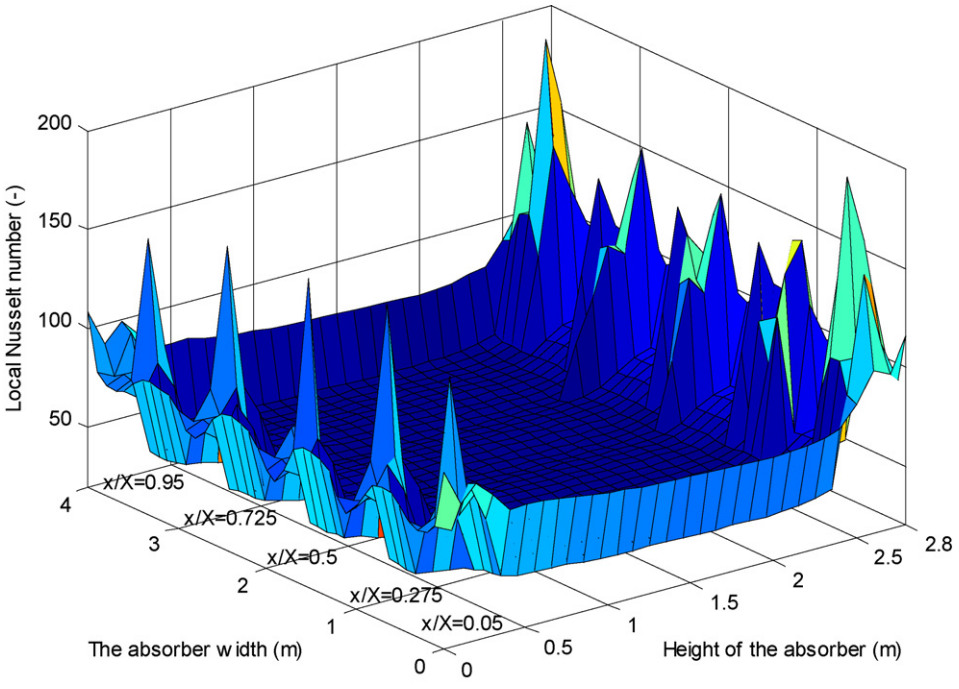

(c)

Fig. 5. (*Continued*.)

to Fohanno and Polidori, the average Nusselt number can be written as $Nu_Y = 0.595(Ra_Y)^{1/5}$ for laminar regime (modified Rayleigh number based on the cavity height $(Ra_Y) \leqslant 6.3 \times 10^9$). It must be considered that when Nusselt number is calculated, the boundary condition for the glass surface is considered as insulated in theoretical calculations, and as convection in numerical calculations. The numerical Nusselt number is higher than the theoretical Nusselt number with an exception for before 8 am and after 17 pm (Fig. 6). This is most probably due to the difference of the boundary and initial conditions since theoretical Nusselt number is also valid for steady-state natural convection. On the contrary, the numerical Nusselt number is valid for unsteady natural convection. For this reason, initial conditions change always depending on previous time step in the numerical calculations.

Distribution of the average velocity in the cavity is given at $y = 0.3$ m (top boundary of the inlet vents), $y = 1.4$ m and $y = 2.5$ m (bottom boundary of the outlet vents) in Fig. 7(a).

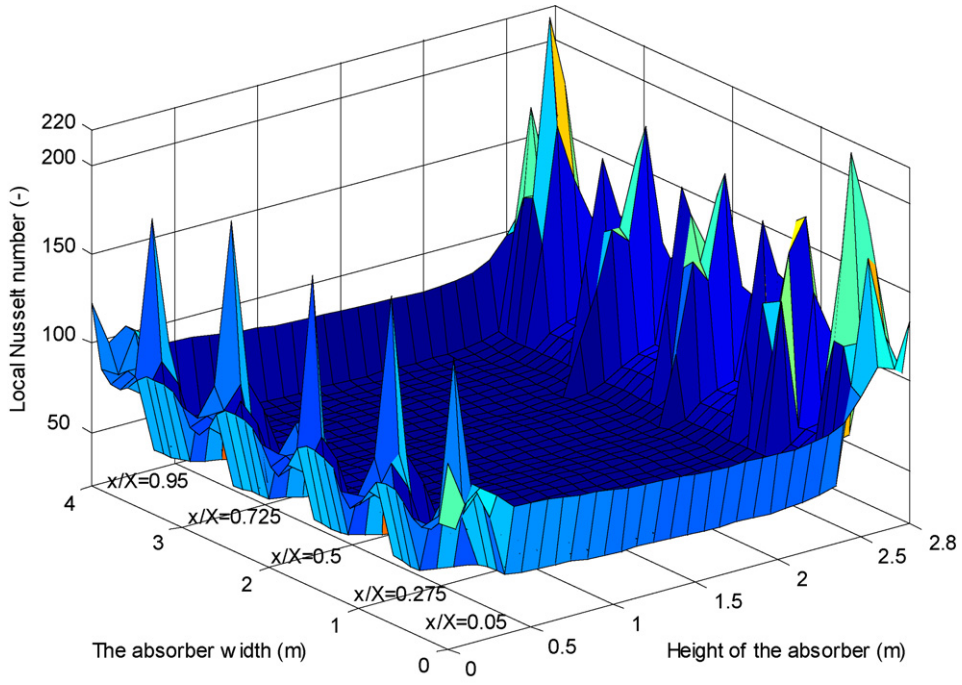

(d)

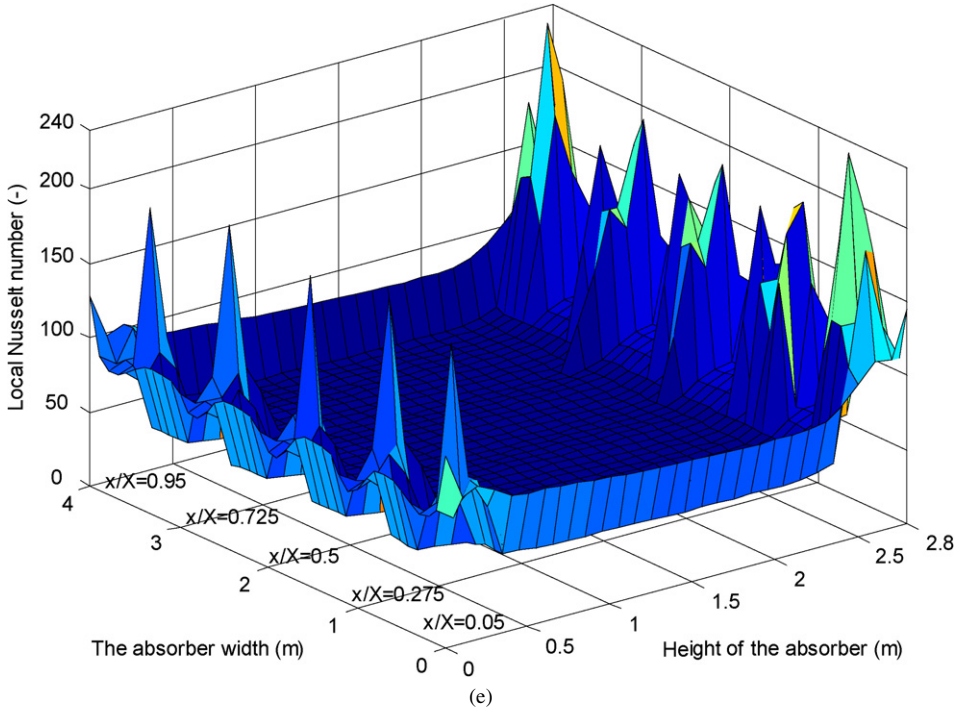

(e)

Fig. 5. (*Continued*.)

The air entered from the room to the cavity goes through the z-direction, and it is nearly constant through z-direction ($0.1\ \mathrm{m\,s^{-1}}$). $y = 1.4$ m indicates the middle of the cavity height. Here, the average velocity distribution of the air differs from that of $y = 0.3$. It is seen that the maximum values of the average velocity are 0.27, 0.04 and $0.11\ \mathrm{m\,s^{-1}}$ on the glass, at the middle of the cavity and on the absorber, respectively. It is also seen that the average velocity of the air increases to the direction of the vents and also on the absorber side. At $y = 2.5$ m, although the velocity distribution is similar to that of $y = 1.4$ m, the velocity is higher than that of $y = 1.4$ m on the absorber side, and is less than that of $y = 1.4$ m on the side of the glass. Likewise, the effect of the vents decreases on the absorber and the glass side.

v-component in y-direction of the average velocity presented in Fig. 7(a) is given in Fig. 7(b). v-component goes forward rather slowly to the direction of the vents. On the side of the absorber, v-component between vents is $0.11\ \mathrm{m\,s^{-1}}$

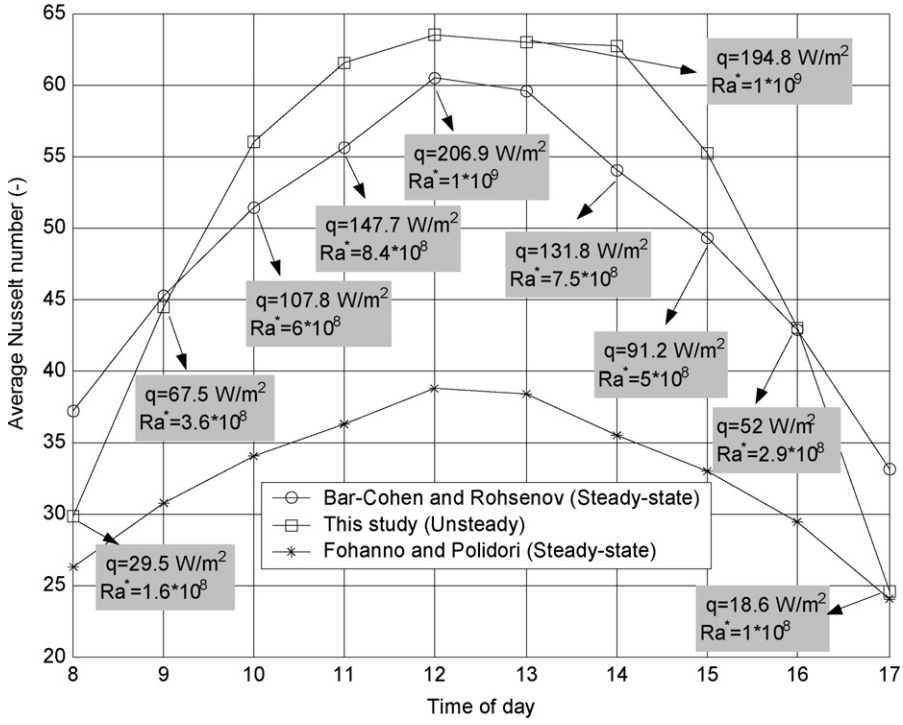

Fig. 6. Changing of average Nusselt number with daytime.

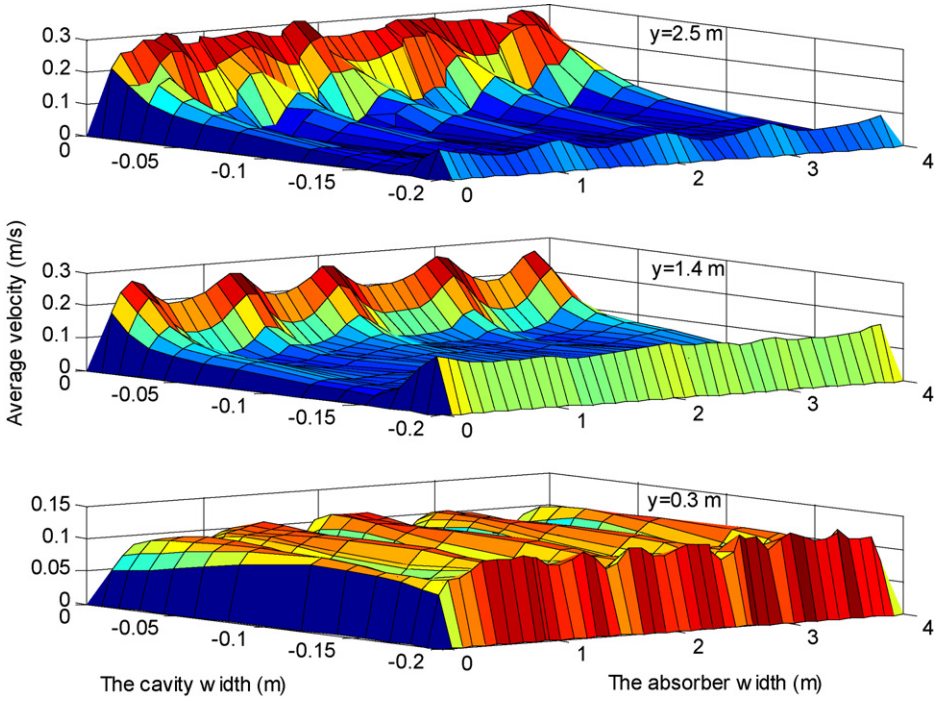

(a)

Fig. 7. Distribution of velocity in the cavity at 8 am for $U_g = 2.6\ \mathrm{W\,m^{-2}\,K^{-1}}$. (a) average velocity, (b) v-component, (c) w-component.

to positive (upper) direction. Because of cooling of the glass, v-component increases up to 0.17 m s^{-1} to the negative (down) direction on the side of the glass. It is seen that the glass surface temperature is less than the initial temperature (6 °C) at $y = 0.3$ m. The heat, in the other words, transfers from the glass to the environment. The direction of the average velocity is completely y-direction at $y = 0.3$ m on the side of the glass except for the side of the absorber. Likewise, v-component is the positive direction on the side of the absorber, and is the negative direction on the side of the glass. The direction of the average velocity is completely y-direction at $y = 1.4$ m and $y = 2.5$ m.

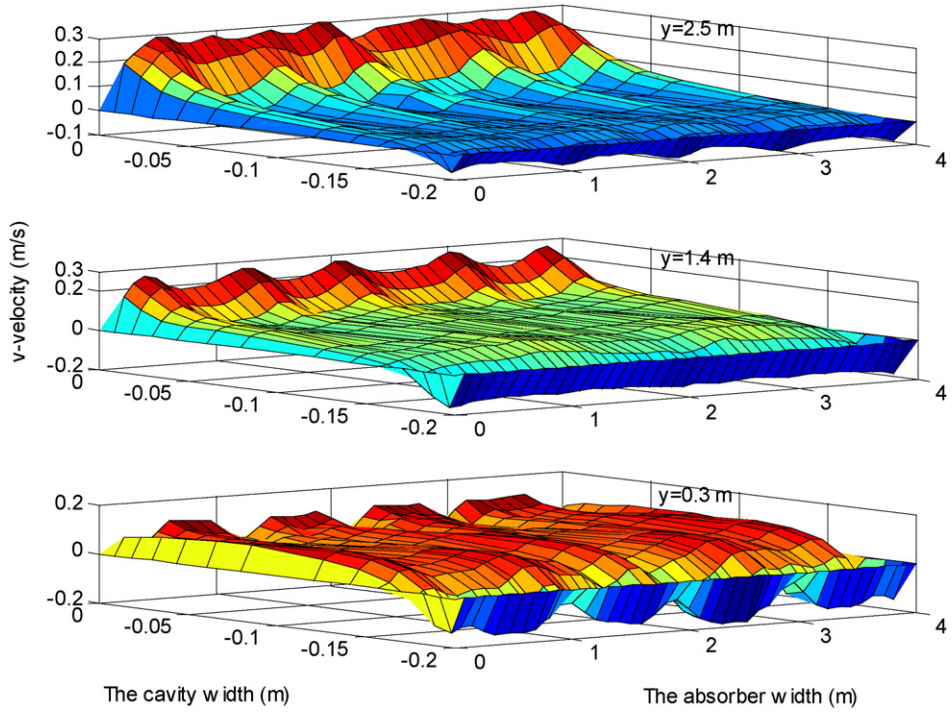

(b)

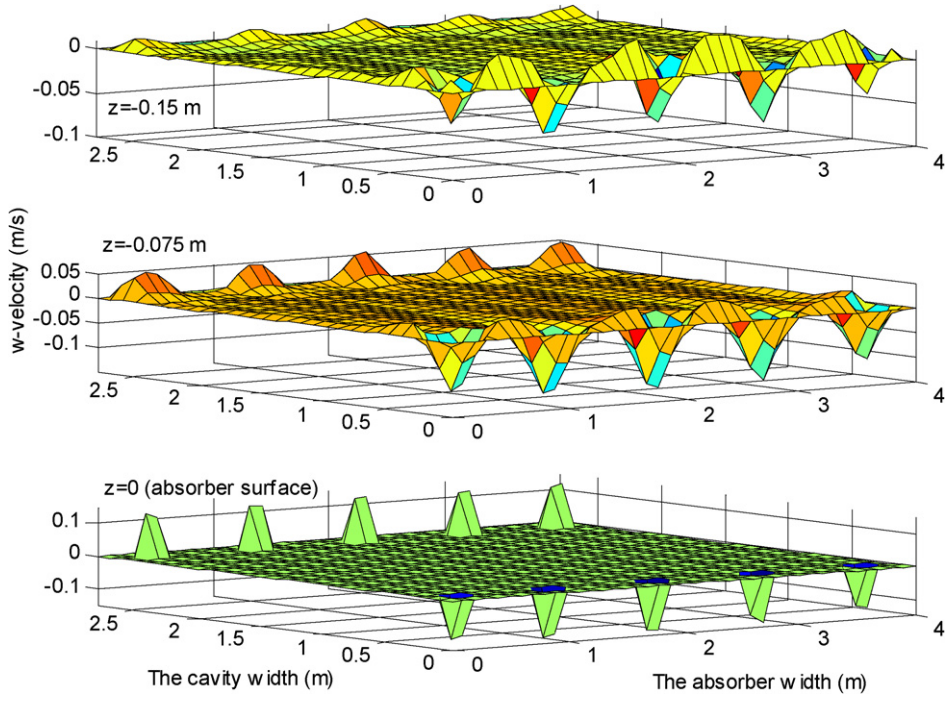

(c)

Fig. 7. (*Continued*.)

Distribution of w-component (z-direction) on the absorber, at $z = -0.075$ m and $z = -0.15$ m is given in Fig. 7(c). When the geometry was formed by Gambit, origin was chosen at the corner of the absorber (Fig. 1). Because of this, minus sign used for lengths must not be considered. As seen from Fig. 7(a) and (b), air velocity is zero on the absorber. The average velocity is completely z-direction at the entrance of the outlet vents and at the exit of the inlet vents. w-components, at the inlet and outlet vents, are approximately equal to each other and each of the w-component value increases from 0.12 to 0.15 m s^{-1}. While w-component in the middle vent ($x/X = 0.5$) is -0.136 m s^{-1}, it decreases up to -0129 m s^{-1} at $x/X = 0.95$ in the inlet vents. Likewise, while w-component in the middle vent is 0.15 m s^{-1}, it decreases up to 0.126 m s^{-1} at

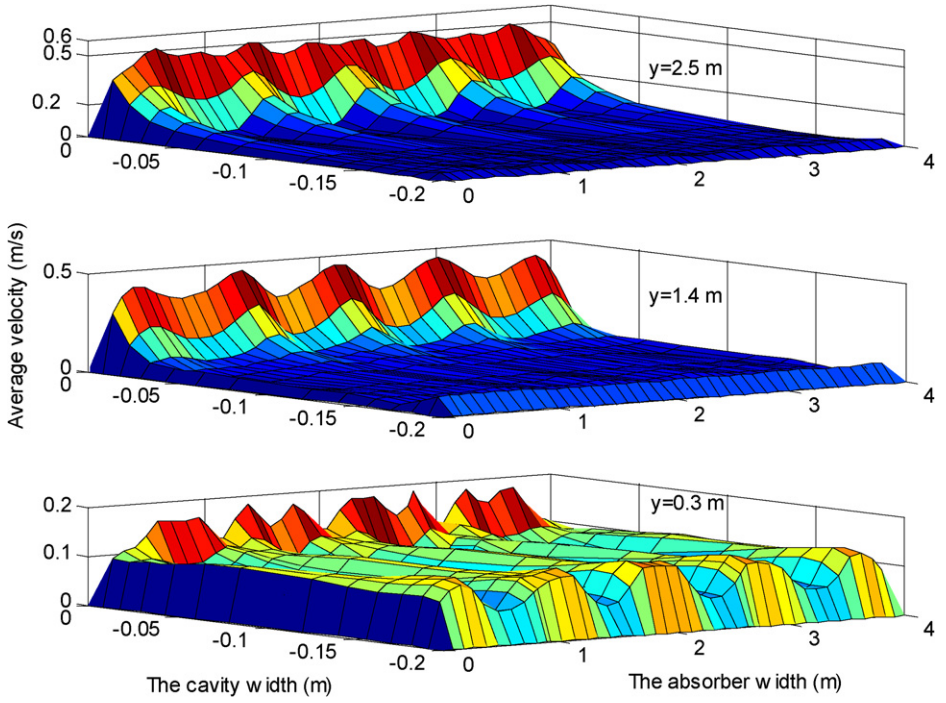

(a)

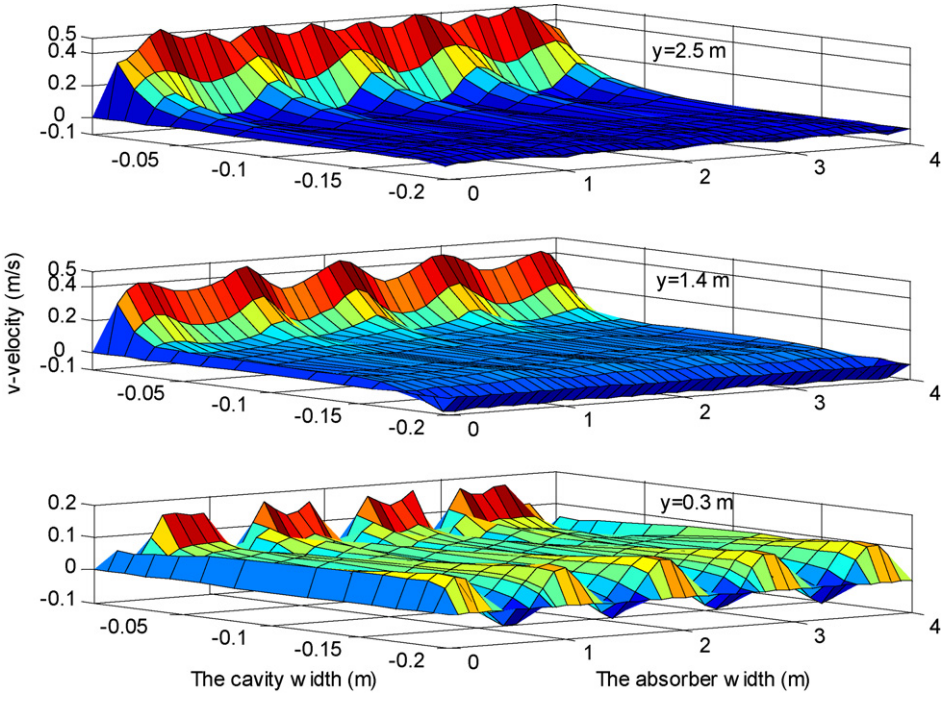

(b)

Fig. 8. Distribution of velocity in the cavity at 10 am for $U_g = 2.6\ \mathrm{W\,m^{-2}\,K^{-1}}$. (a) average velocity, (b) v-component, (c) w-component.

the $x/X = 0.05$ and $x/X = 0.95$. The effect of outlet vents on the w-component decreases up to $0.05\ \mathrm{m\,s^{-1}}$ at $z = -0.075$ m (Fig. 7(c)). w-component decreases up to $10^{-4}\ \mathrm{m\,s^{-1}}$, except for the direction of the vents.

The air velocity increases depending on the daytime and the heat flux consequently. Even though the velocity of the air increases depending on the heat flux, distribution of the air velocity in the cavity is similar to each other in view. The average velocity, v-component and w-component are given in Fig. 8 (a), (b), (c) at 10 am, respectively. These velocities increase up to $0.7\ \mathrm{m\,s^{-1}}$ at 12 am as seen from Fig. 9 (a), (b), (c).

In this study, three different overall heat transfer coefficients (U_g) of the glass on which convection boundary condition is applied were evaluated for $T_e = 0\,^{\circ}\mathrm{C}$. As known, overall heat transfer coefficients of multi-layer glass change depending on the fluid properties between the glasses and the glass thickness.

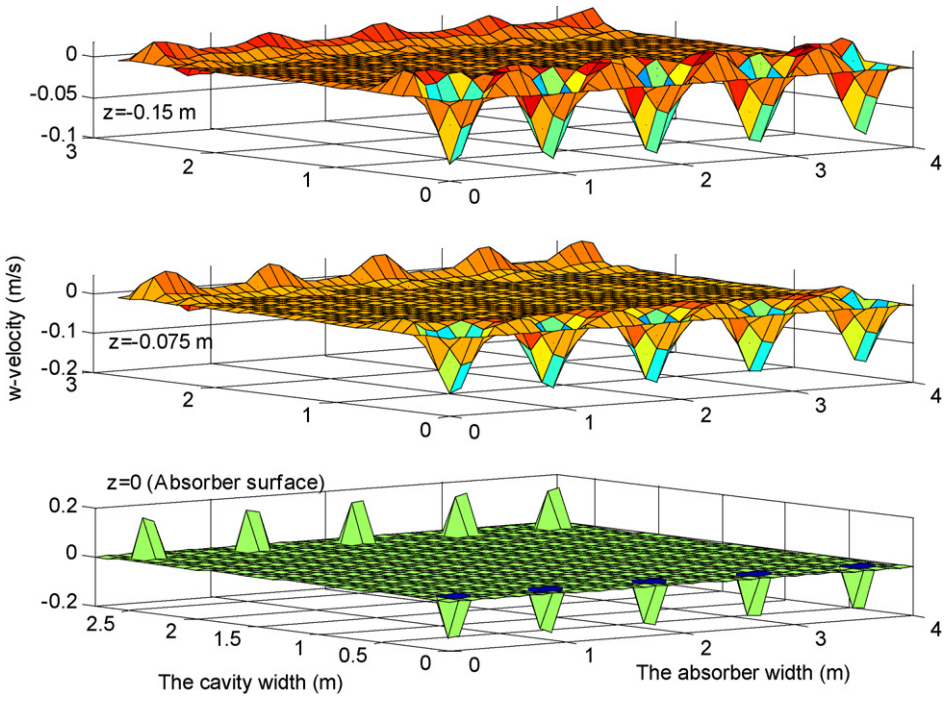

(c)

Fig. 8. (*Continued*.)

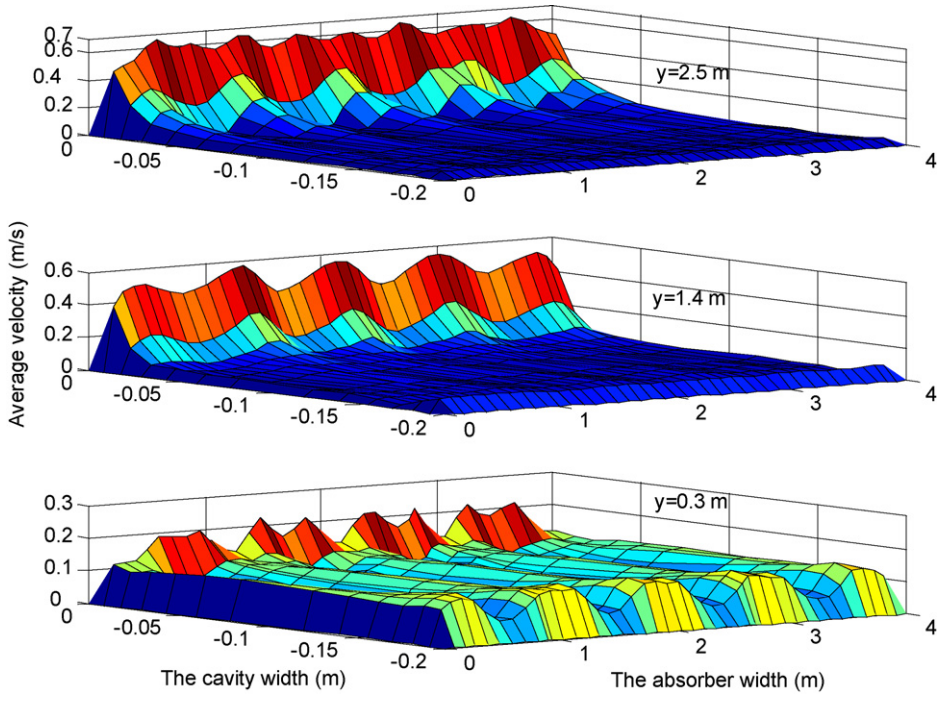

(a)

Fig. 9. Distribution of velocity in the cavity at 12 am for $U_g = 2.6\ \mathrm{W\,m^{-2}\,K^{-1}}$. (a) average velocity, (b) v-component, (c) w-component.

The air is generally used as a fluid filled between the glasses; but, Argon and Krypton can also be preferred for some special cases. The overall heat transfer coefficients of the glass can change between 1.2 and 3 $\mathrm{W\,m^{-2}\,K^{-1}}$ depending on the glass thickness, the gap between the glasses or the working fluid. In this work, overall heat transfer coefficients are arbitrarily chosen among the values given by TS 825 (Turkish Standards) for the double glass. According to Eq. (9), U_g is proportional to the heat transfer. In this case, heat losses increase depending on U_g and temperature differences $(T_g - T_e)$. The changing of the heat loss with the daytime is given in Fig. 10 for each U_g value. As shown in Fig 10, heat loss is 108.55, 108.3 and 106.1 W for

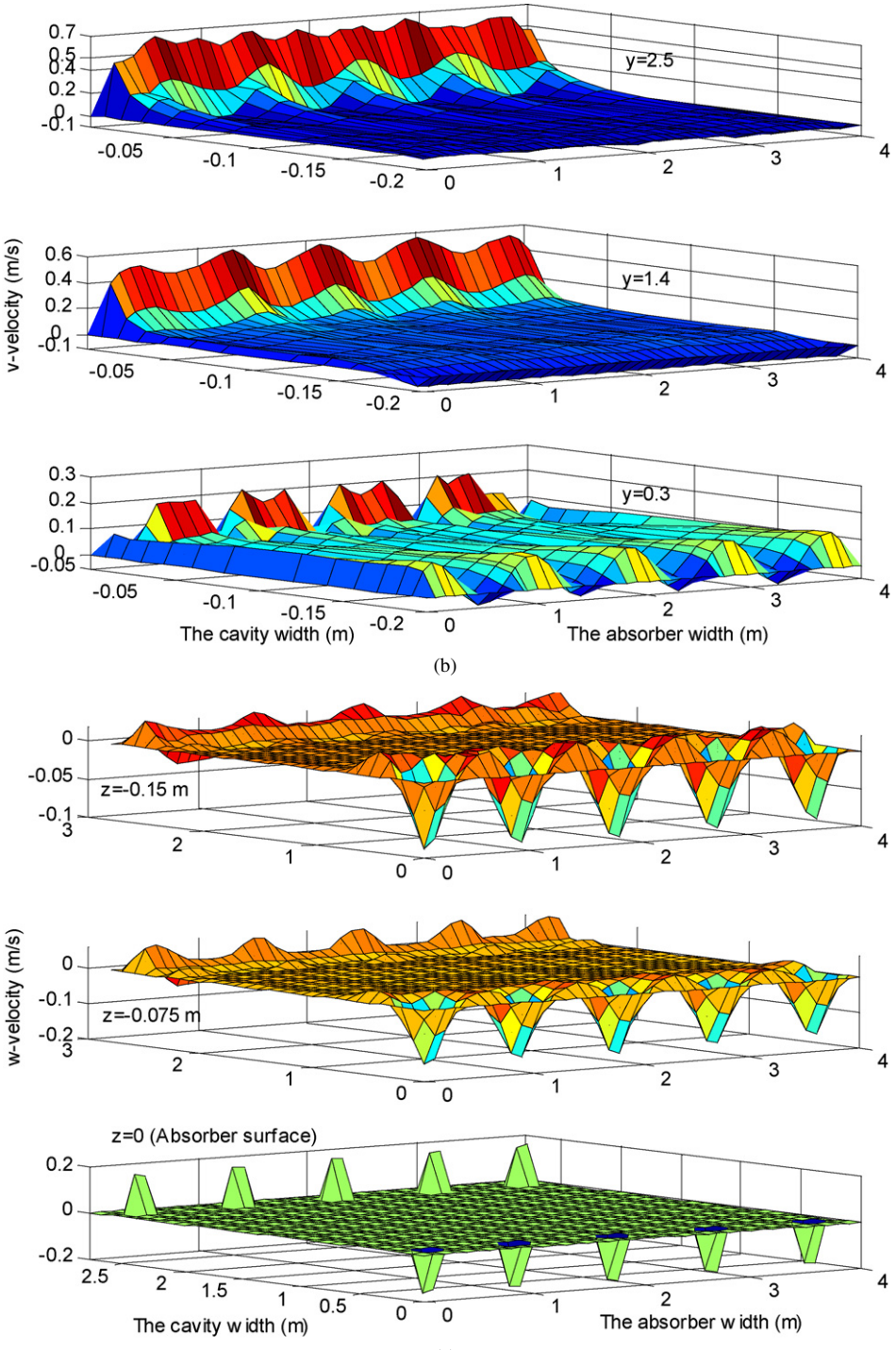

(b)

(c)

Fig. 9. (*Continued*.)

U_g values of 2.6 2 and 1.6 $\mathrm{W\,m^{-2}\,K^{-1}}$ at 8 am, respectively. Since average solar radiation increases up to 67.51 $\mathrm{W\,m^{-2}}$ at 9 am, the glass surface temperature increases. The heat loss increases 60.1% for 2.6 $\mathrm{W\,m^{-2}\,K^{-1}}$, 28.4% for 2 $\mathrm{W\,m^{-2}\,K^{-1}}$ and 8.07% for $\mathrm{W\,m^{-2}\,K^{-1}}$ according to previous time step. After 9 am, the increment of the heat loss decreases for U_g of 2.6 and 2 $\mathrm{W\,m^{-2}\,K^{-1}}$. The increment ratio has the same gradient at each time step for $U_g = 1.6\ \mathrm{W\,m^{-2}\,K^{-1}}$. The heat loss increases and reaches the maximum in the midday.

In this study, the average velocity of the air in the outlet vents is maximum in the middle vents and it decreases away from the middle vents. Changing of the average velocity of the air in the vents is given in Fig. 11 for 8, 10 and 12 am. The average velocity of the air increases approximately up to 0.15 $\mathrm{m\,s^{-1}}$ in the middle vent at 8 am., 0.175 $\mathrm{m\,s^{-1}}$ at 10 am, and 0.19 $\mathrm{m\,s^{-1}}$ at 12 am. Changing of total mass flow rate in outlet vents with daytime is also given in Fig. 11 for $U_g = 2.6\ \mathrm{W\,m^{-2}\,K^{-1}}$ and $T_e = 0\,^{\circ}\mathrm{C}$. The mass flow rate is approximately 0.025 $\mathrm{kg\,s^{-1}}$

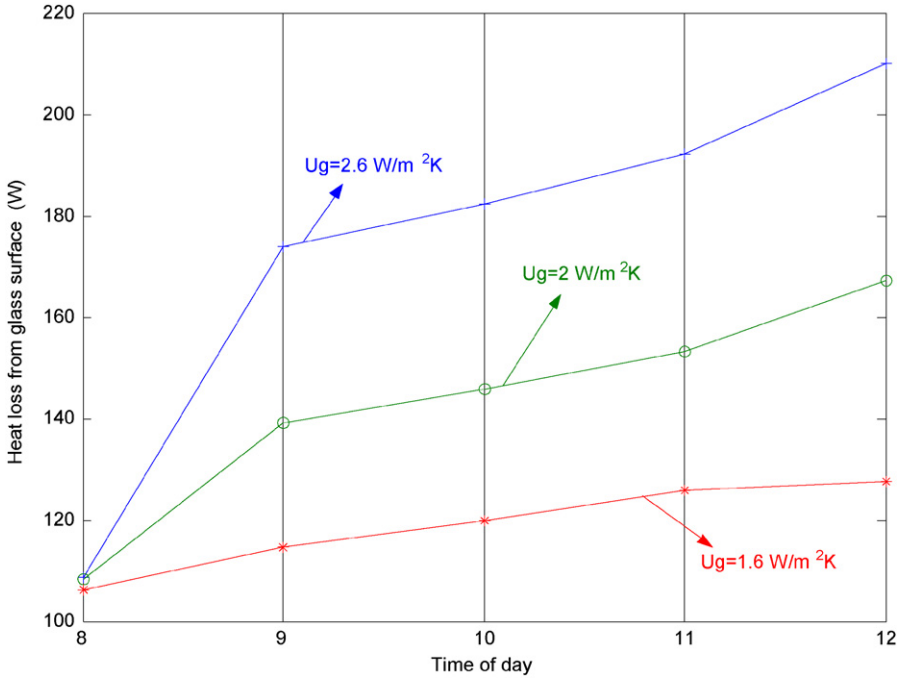

Fig. 10. Changing of heat loss from the glass surface with daytime for each U_g value.

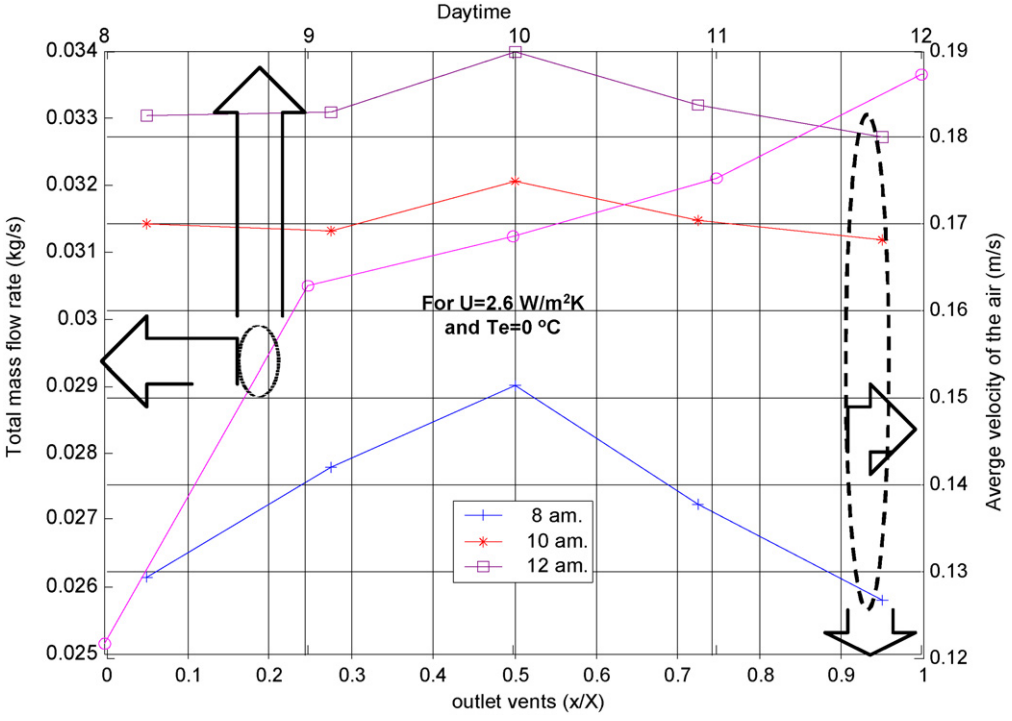

Fig. 11. Changing of mass flow rate and average velocity of the air with daytime and outlet vents, respectively.

at 8 am. Then it increases up to 0.034 kg s^{-1} depending on the heat flux on the SAW.

The effect of U_g on Nusselt number is given in Fig. 12. The most important parameter on Nusselt number is Rayleigh number for each U_g values. However, the effect of U_g on Nusselt number is to be more in low Rayleigh number. Nusselt number for U_g values of 2.6, 2 and 1.6 W m^{-2} K^{-1} is 29.84, 35.95 and 37.41 in $Ra = 1.6 \times 10^8$, respectively. Considering this, when U_g decreases from 2.6 to 2 W m^{-2} K^{-1}, Nusselt number increases 20.47%, and also decreasing results in a 4% increase from 2 to 1.6 W m^{-2} K^{-1}. Therefore, we can conclude that the increment rate of Nusselt number decreases in the case of decreasing U_g value. For $U_g = 2.6$ W m^{-2} K^{-1} and $Ra = 1.1 \times 10^9$ Nusselt number is 63.46, and for the same Rayleigh number and $U_g = 1.6$ W m^{-2} K^{-1} it is 64.23.

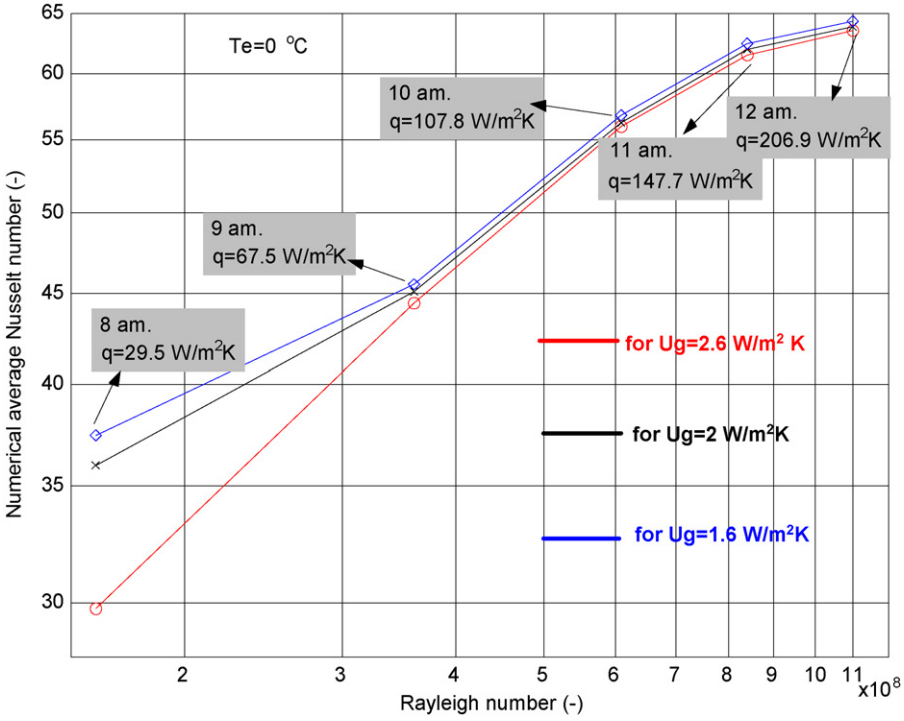

Fig. 12. Changing of average Nusselt number with Rayleigh number.

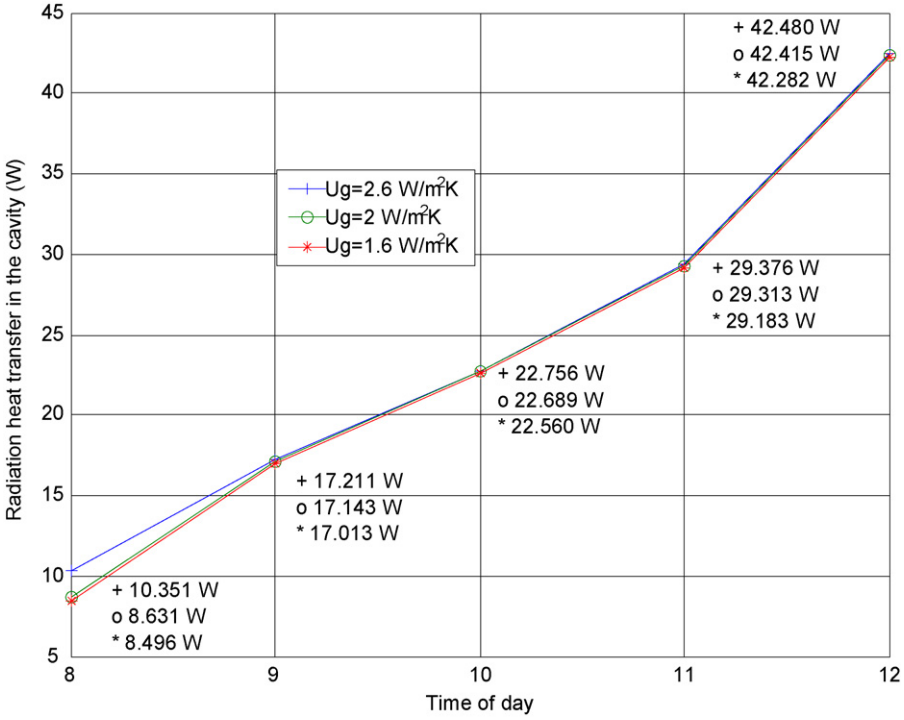

Fig. 13. Changing of radiation heat transfer in the cavity with daytime.

A correlation was derived using multiple regressions for Nusselt number given in Fig. 12.

$$Nu = 0.1.Ra^{0.32}.(U.S/k)^{-0.068} \quad (R = 0.976) \tag{8}$$

The empirical formula given above is valid for unsteady natural convection since heat flux changes between 29.5 and 206.9 W m^{-2} K^{-1} and Rayleigh number is in the range of 10^8 and 10^9. The effect of U_g on the heat transfer via radiation is given in Fig. 13. Because the effect of U_g on the heat transfer via radiation is less significant, the heat transfer values for each parameter are presented in Fig. 13 showing also the data with three digits after decimal point. Similar to Nusselt number, the most important parameters on the radiation heat transfer is heat flux (q), and Rayleigh number. Heat transfer, on the other hand,

decreases contrary to Nusselt number if U_g is decreased. The local temperature values are used to calculate the radiation heat transfer defined below:

$$Q_R = \frac{\sigma.}{\frac{1}{\varepsilon_1}+\frac{1}{\varepsilon_2}-1}.\int_A (T^4_{a(i,j)} - T^4_{g(i,j)}).\mathrm{d}A \tag{9}$$

where σ is Stefan–Boltzmann constant given as $5.67 \times 10^{-8}\ \mathrm{W\,m^{-2}\,K^{-4}}$, ε is emissivities of the surfaces. As known, in the case of decreasing U_g, the glass surface temperature increases, and so the radiation heat transfer decreases. It is seen from Fig. 13 that the radiation heat transfer increases approximately 98% when Rayleigh number is increased from 1.6×10^8 to 3.6×10^8 at 8 am. However, the radiation heat transfer increases 22.3% in the case of increasing U_g from 1.6 to $2.6\ \mathrm{W\,m^{-2}\,K^{-1}}$.

4. Conclusions

In this study, by considering the cavity of the passive heating room, unsteady state heat transfer and flow equations were solved numerically. Two types of the heat transfer boundary conditions are prescribed as convection and variable heat flux on the side of the glass and the absorber. As for the others, boundary conditions are chosen as constant temperature and convection.

We can conclude from the above discussions that the heat flux and the overall heat transfer coefficient (U_g) of the glass have important effects on the heat transfer. It is seen that the average velocity of the air changes depending on the vent locations. While the average velocity of the air is the maximum in the middle vents, it decreases away from the middle vents. Total mass flow rate, which is addition of mass flow rate in each inlet or outlet vent, is $0.0251\ \mathrm{kg\,s^{-1}}$ for $Ra = 1.1 \times 10^8$ at 8 am, and it increases up to $0.0336\ \mathrm{kg\,s^{-1}}$ in the midday depending on Rayleigh number. The overall heat transfer coefficient for low Rayleigh number affects the average Nusselt number more than that for high Rayleigh number. In this work, local Nusselt number and velocities are given as three dimensional (3-D) in the cavity. With this work is anticipated to be a leader for further studies, which will be done on the augmentation of the effectiveness of the passive heating systems. Because of obtaining local velocity components, some required manipulations were executed to avoid the heat losses and dead locations in the cavity. For instance, the heat loss from the cavity to the environment is to be more in the neighborhood of the inlet vents. By this definition, a certain part of the glass surface can be insulated depending on certain condition.

Acknowledgement

The authors thank İstanbul Technical University for using of Fluent 5.5.

References

[1] L. Buzzoni, R. Dali'Olio, M. Spiga, Energy analysis of a passive solar system, Rev. Gen. Therm. 37 (1998) 411–416.
[2] G. Data, Effect of fixed horizontal louver shading devices on thermal performance of building by TRNSYS simulation, Renewable Energy 23 (2001) 497–507.
[3] G. Ballestini, M. De Carli, N. Masiero, G. Tombola, Possibilities and limitations of natural ventilation in restored industrial archaeology buildings with a double-skin façade in Mediterranean climates, Building and Environment 40 (7) (2005) 983–995.
[4] W. Chen, W. Liu, Numerical analysis of heat transfer in a composite wall solar-collector system with a porous absorber, Appl. Energy 78 (2004) 137–149.
[5] J. Khedari, N. Rachapradit, J. Hirunlabh, Field study of performance of solar chimney with air-conditioned, Energy 28 (11) (2003) 1099–1114.
[6] X.Q. Zhai, Y.J. Dai, R.Z. Wang, Comparison of heating and natural ventilation in a solar house induced by two roof soar collectors, Appl. Thermal Engrg. 25 (5–6) (2005) 741–757.
[7] J. Hirunlabh, W. Kongduang, P. Namprakai, J. Khedari, Study of natural ventilation of houses by a metallic solar wall under tropical climate, Renewable Energy 18 (1999) 109–119.
[8] R.B. Yedder, E. Bilgen, Natural convection and conduction in Trombe wall systems, Int. J. Heat Mass Transfer 34 (1991) 1237–1248.
[9] F. Mootz, J. Bezian, Numerical study of a ventilated facade panel, Solar Energy 57 (1996) 29–36.
[10] Z. Zrikem, E. Bilgen, Theoretical study of a non-convective Trombe wall collector with honeycomb structure, Solar & Wind Technology 3 (1986) 33–44.
[11] M. Hasnaoui, Z. Zrikem, P. Vasseur, E. Bilgen, Solar radiation induced natural convection in enclosures with conducting walls, Solar & Wind Technology 7 (1990) 515–525.
[12] F.N. Demirbilek, U.G. Yalçıner, A. Ecevit, E. Sahmali, M. Inanici, Analysis of the thermal performance of a building design located at 2465 m: Antalya-Saklikent national observatory guesthouse, Building and Environment 38 (1) (2003) 177–184.
[13] G. Gan, S.B. Riffat, A numerical study of solar chimney for natural ventilation of building with heat recovery, Appl. Thermal Engrg. 18 (12) (1998) 1171–1187.
[14] J. Rincon, N. Almao, E. Gonzalez, Experimental and numerical evaluation of a solar cooling system under hot and humid climatic conditions, Solar Energy 71 (1) (2001) 71–80.
[15] A.M. Rodrigues, A.C. Piedade, A. Lahellec, J.Y. Grandpeix, Modeling natural convection in a heated vertical channel for room ventilation, Building and Environment 35 (2000) 455–469.
[16] R. Letan, V. Dubovsky, G. Ziskind, Passive ventilation and heating by natural convection in a multi-storey building, Building and Environment 38 (2003) 197–208.
[17] İ. Kurtbaş, Investigation of applicability of Trombe wall in Elazıg conditions, PhD Thesis, Firat University, Elazıg, Turkey, 2005.
[18] S. Kazansky, V. Dubovsky, G. Ziskind, R. Letan, Chimney-enhanced natural convection from a vertical plate: Experiments and numerical simulations, Int. J. Heat Mass Transfer 46 (2003) 497–512.
[19] FLUENT User's Guide, Version 5.5, Fluent Incorporated.
[20] J.A. Duffie, W.A. Beckman, Solar Engineering of Thermal Processes, John Wiley, New York, 1991.
[21] S.K.W. Tou, C.P. Tso, X. Zhang, 3-D numerical analysis of natural convective liquid cooling of a 3 × 3 heater array in rectangular enclosures, Int. J. Heat Mass Transfer 42 (1999) 3231–3244.
[22] F.P. Incropera, D.P. DeWitt, Fundamentals of Heat and Mass Transfer, fourth ed., John Wiley, New York, 1996.
[23] S. Fohanno, G. Polidori, Modelling of natural convection heat transfer at an internal surface, Energy and Building 38 (2006) 548–553.